

Edge state transport through disordered graphene nanoribbons in the quantum Hall regime

Fabian Duerr,¹ Jeroen B. Oostinga,^{1,*} Charles Gould,¹ and Laurens W. Molenkamp¹

¹*Physikalisches Institut (EP3), University of Würzburg, Am Hubland, D-97074, Würzburg, Germany*

(Dated: September 16, 2018)

The presence of strong disorder in graphene nanoribbons yields low-mobility diffusive transport at high charge densities, whereas a transport gap occurs at low densities. Here, we investigate the longitudinal and transverse magnetoresistance of a narrow (~ 60 nm) nanoribbon in a six-terminal Hall bar geometry. At $B = 11$ T, quantum Hall plateaux appear at $\sigma_{xy} = \pm 2e^2/h$, $\pm 6e^2/h$ and $\pm 10e^2/h$, for which the Landau level spacing is larger than the Landau level broadening. Interestingly, the transport gap does not disappear in the quantum Hall regime, when the zero-energy Landau level is present at the charge neutrality point, implying that it cannot originate from a lateral confinement gap. At high charge densities, the longitudinal and Hall resistance exhibit reproducible fluctuations, which are most pronounced at the transition regions between Hall plateaux. Bias-dependent measurements strongly indicate that these fluctuations can be attributed to phase coherent scattering in the disordered ribbon.

PACS numbers: 73.23.-b, 72.80.Vp, 73.43.Qt

Since the discovery of graphene [1], the investigation of transport through low-dimensional graphene structures, such as nanoribbons and quantum dots, has obtained much attention [2]. Whereas graphene is a gapless material system, size quantization effects in narrow structures are expected to open a bandgap [3]. Moreover, depending on the precise edge structure and interaction effects, peculiar edge states are predicted to appear [3, 4]. Transport measurements on ribbons have shown, however, that the presence of bulk and edge disorder obscures the observability of bandgap and edge state related transport properties [2].

Strong edge disorder gives rise to enhanced intervalley scattering in narrow ribbons [5]. This results in a suppression of the carrier mobility in the high-density regime, and the occurrence of a transport gap in the low-density regime. A transport gap appears due to the confinement of charges, for which different origins have been proposed, e.g., the occurrence of a strong localization regime [6] or the presence of disorder-induced electron and hole puddles which are separated by a bandgap [7]. At high density, the charge carriers are delocalized and propagate diffusively through a disordered ribbon. Although transport through magnetoelectric subbands has been predicted in narrow ribbons with well-defined edges [8], experiments have shown that the presence of strong disorder impedes the occurrence of conductance quantization at zero magnetic field [9] and the development of quantum Hall edge states at high field [10]. Profound knowledge of disorder effects on transport is therefore needed to get a better understanding of the electronic properties of low-dimensional graphene structures.

Here we present a systematic study of electronic transport through a 60 nm wide graphene nanoribbon in a six-terminal Hall bar geometry. Our transport measurements show that the transport gap at low charge den-

sity does not disappear in the quantum Hall regime, and therefore, shows that a bandgap due to lateral confinement does not play a crucial role in the formation of the transport gap at high magnetic field. Outside the transport gap, the measurements at the highest applied magnetic field ($B = 11$ T) only reveal the quantum Hall plateaux at $\sigma_{xy} = \pm 2e^2/h$, $\pm 6e^2/h$ and $\pm 10e^2/h$, for which the corresponding Landau level spacing is larger than the estimated Landau level broadening. Moreover, the longitudinal and Hall resistance exhibit aperiodic fluctuations, which are most pronounced in the transition regions between the quantum Hall plateaux. Since these reproducible fluctuations are strongly suppressed when the bias and thermal energy are larger than the estimated Thouless energy, they can be mainly attributed to quantum interference effects in the disordered ribbon.

Exfoliated single-layer graphene flakes are transferred to a highly p-doped Si substrate containing a 285 nm SiO₂ top layer. After deposition of Ti/Au electrodes onto the graphene, the flakes are etched in an Ar/O₂ plasma to obtain narrow nanoribbons (width $\lesssim 100$ nm) in a six-terminal Hall bar geometry (Fig. 1a). The etched structures are cleaned at 200°C in forming gas to reduce the amount of contamination at the graphene surface. The transport experiments are carried out in an Oxford dilution refrigerator at temperatures of 30 mK and 4.2 K. The longitudinal and transverse resistance are measured as function of current bias (I_{bias}), gate-voltage (V_g) and magnetic field (B) by using standard lock-in detection techniques. We discuss the data of a device consisting of a ribbon with length $L = 250$ nm and width $W = 60$ nm (these data are representative for the other measured devices of similar dimensions).

First we discuss the transport characteristics of the device at $T = 4.2$ K. The differential conductance ($G = dI/dV_{xx}$) versus gate voltage (Fig. 1b) clearly shows

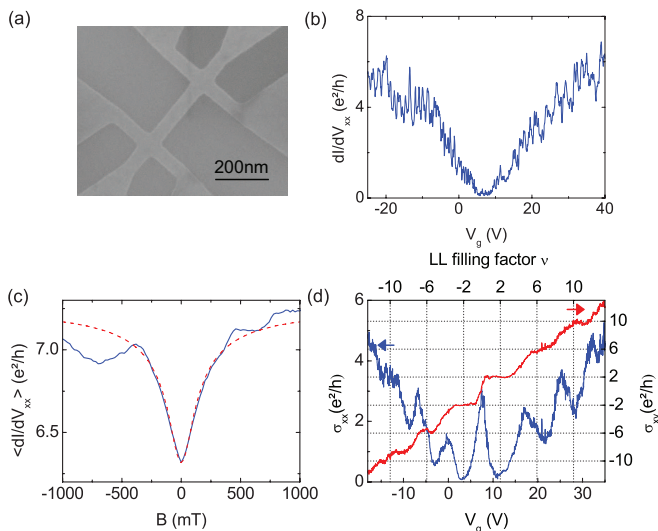


FIG. 1: (a) Scanning electron micrograph of a six-terminal graphene nanoribbon device. (b) dI/dV_{xx} versus V_g at $B = 0$ T. (c) Ensemble average of dI/dV_{xx} versus B , determined at high hole densities in the range of $n \approx (4-6) \cdot 10^{12} \text{ cm}^{-2}$. The dashed line is a fit of the weak localization theory (Eq. 12 of Ref. [14]) to the data with the phase coherence length as only fitting parameter, yielding $l_\phi \approx 100$ nm. (d) σ_{xx} and σ_{xy} versus V_g at $B = 11$ T. The gate-voltage dependence of the LL filling factor is: $\nu = \frac{h}{e^2 B} C_g (V_g - V_g^D)$. All data are measured at $T = 4.2$ K.

a suppressed conductance at low density in the vicinity of the Dirac point ($V_g^D \approx 7.5$ V), as is characteristic for graphene nanoribbon devices [2]. At high electron ($V_g > 10$ V) and hole density ($V_g < 5$ V), we observe reproducible conductance fluctuations. In this regime, the field-effect mobility of the charge carriers is $\mu = \frac{L}{WC_g} \frac{dG}{dV_g} \approx 1500 \text{ cm}^2/\text{Vs}$ where $C_g \approx 210 \text{ } \mu\text{F}/\text{m}^2$ is the effective gate capacitance [11]. This corresponds to a diffusion constant of $D = \frac{L}{W} \frac{G}{\nu e^2} \approx 0.01 \text{ m}^2/\text{s}$ and a mean free path of $l_m = 2D/\nu_f \approx 20 \text{ nm}$ (where ν is the density of states and $\nu_f \approx 10^6 \text{ m/s}$ is the Fermi velocity). Such small values of the mobility, diffusion constant and mean free path are typical for plasma-etched graphene nanoribbon devices, and are a consequence of the high amount of disorder in these systems [2, 6, 7].

To investigate the occurrence of weak localization in the diffusive transport regime, we measure the low-field magnetoconductance at different gate voltages corresponding to high hole densities. Since each individual measurement at constant charge density exhibits reproducible conductance fluctuations, we determine the ensemble average of measurements at different charge densities (Fig. 1c). The averaged magnetoconductance versus magnetic field clearly shows a weak localization correction of $\sim e^2/h$, indicating the occurrence of strong intervalley scattering, as expected in disordered ribbons with short-range disorder at the edges [12]. A fit of the weak localization theory for graphene nanoribbons (i.e.,

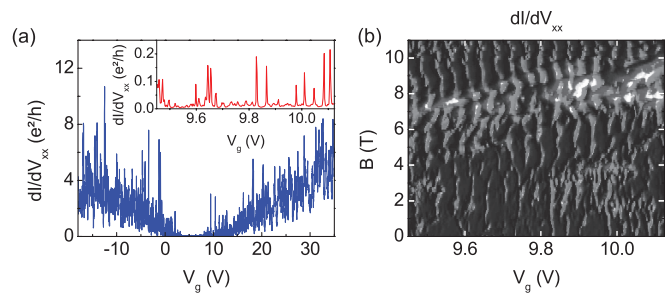


FIG. 2: (a) dI/dV_{xx} versus V_g at $B = 0$ T. Inset: dI/dV_{xx} versus V_g in a small V_g range in the transport gap, showing regions of suppressed dI/dV_{xx} and conductance peaks. (b) dI/dV_{xx} versus V_g and B . The black regions correspond to suppressed dI/dV_{xx} and the grey/white regions correspond to regions where dI/dV_{xx} is not suppressed (conductance peaks). All data are measured at $T = 30$ mK.

eq. 12 of Ref. [14]) to our low-field magnetoconductance data yields a phase coherence length of $l_\phi \approx 100$ nm (see dashed line in Fig. 1c). This shows that electronic transport at high carrier densities is in the diffusive phase coherent regime (i.e., $l_m < L, W \sim l_\phi$).

Recent experiments on two-terminal graphene nanoribbon devices [10] have shown that edge state transport occurs at very high magnetic fields ($B \gg 10$ T). In order to study edge state transport in graphene nanoribbons more profoundly, we measure the longitudinal ($R_{xx} = dV_{xx}/dI$) and Hall resistance ($R_{xy} = dV_{xy}/dI$) of our six-terminal device at high magnetic fields up to $B = \pm 11$ T, from which we determine the longitudinal (σ_{xx}) and Hall conductivity (σ_{xy}) [13]. We find that the quantum Hall effect is observable at magnetic fields larger than $B \approx 6$ T, as expected if $\mu B \gtrsim 1$. Fig. 1d shows Shubnikov-de Haas (SdH) oscillations of σ_{xx} and quantization steps of σ_{xy} as function of V_g at $B = \pm 11$ T. The Hall plateaux occur at $\sigma_{xy} = \nu e^2/h$ with $\nu = \pm 2, \pm 6$ and ± 10 , which correspond to the characteristic quantization series of Dirac fermions in single-layer graphene [1].

The measurement data show that the $\nu = \pm 2$ plateaux of σ_{xy} are most pronounced. These plateaux occur when the SdH oscillations of σ_{xx} exhibit a minimum value. However, σ_{xx} does not vanish completely, indicating that scattering between states at opposite edges is not fully suppressed. Fig. 1d shows that the $\nu = \pm 6$ and $\nu = \pm 10$ plateaux are less well developed and do not coincide with the minimum values of the SdH oscillations of σ_{xx} . This is probably a consequence of the strong disorder-induced potential fluctuations in the device [2]. The minimum values of σ_{xx} increase with $|\nu|$, indicating an enhancement of scattering between opposite edges for increasing $|\nu|$. In general, σ_{xy} plateaux are well developed if the energy spacing between the corresponding Landau levels (LL) is much larger than the LL broadening (Γ). In graphene, the LL spacing decreases with increasing $|\nu|$, whereas the broadening of the LLs does not vary:

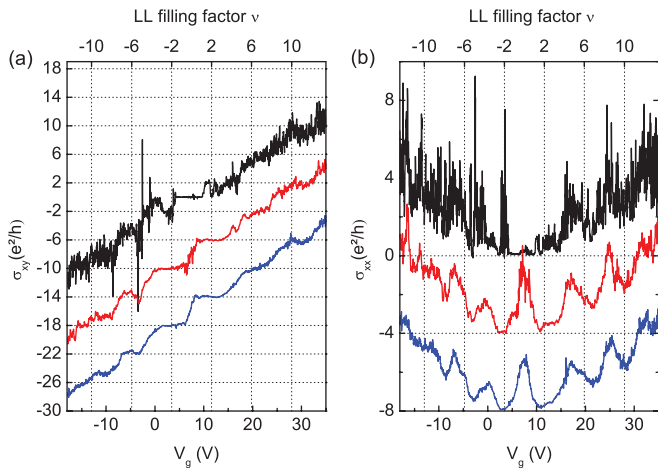


FIG. 3: (a) σ_{xy} and (b) σ_{xx} versus V_g at $B = 11$ T and $I_{bias} = 0$ nA (black), 86 nA (red) and 344 nA (blue). The red and blue curves are shifted with respect to the black curve for clarity. All data are measured at $T = 30$ mK.

$\Gamma \approx \hbar v_f / l_m \approx 30$ meV for each LL. This explains why only the $|\nu| = 2, 6$ and 10 plateaux are visible up to $B = 11$ T with the $\nu = \pm 2$ plateaux as the most pronounced ones [15].

Let us continue the analysis by considering the transport measurements at lower temperature ($T = 30$ mK). In the vicinity of the Dirac point, the conductance measurement versus V_g at zero magnetic field clearly shows a transport gap in a gate-range of $\Delta V_g \approx 8$ V (Fig. 2a). This corresponds to an energy scale of $\Delta E = \hbar v_f \sqrt{2\pi C_g \Delta V_g} / e \approx 160$ meV, which can be attributed to the disorder-induced potential fluctuations in the ribbon [6], possibly in conjunction with a lateral confinement gap [7]. Earlier transport experiments have shown that, in this low-density regime, electrons are confined in small areas of the ribbon [2]. In our conductance measurements, we clearly observe conductance peaks in the transport gap (inset of Fig. 2a), showing that electron states are indeed localized in the low-density regime and transport is dominated by charging effects. By measuring the conductance as function of magnetic field in a small gate-voltage range of the transport gap (Fig. 2b), we observe conductance peaks in the full magnetic field range, including the quantum Hall regime ($B \gtrsim 6$ T). This result shows that electrons are confined at low densities, even when the zero-energy LL appears at the Dirac point. This rules out that a bandgap due to lateral confinement plays a crucial role in the physical mechanism underlying the occurrence of the transport gap at high magnetic field (consistent with [5, 6]), because the zero-energy LL closes such a size quantization gap [16].

At $T = 30$ mK, we observe large reproducible fluctuations of σ_{xx} and σ_{xy} at high charge densities in the quantum Hall regime (Fig. 3a,b), which obscure the visibility of SdH oscillations of σ_{xx} and quantization plateaux

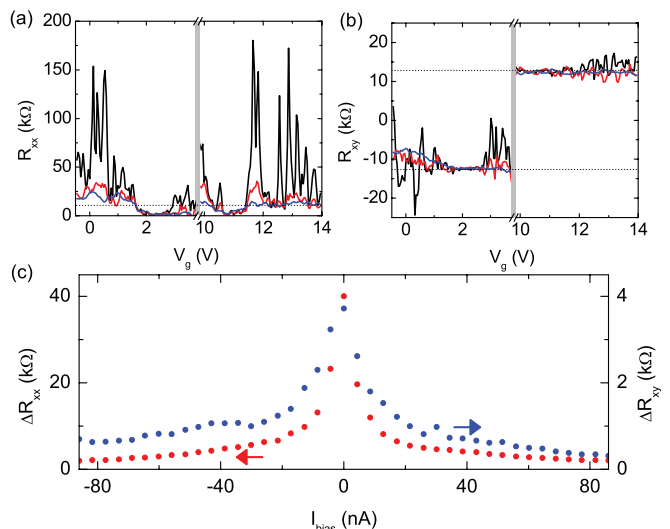


FIG. 4: (a) R_{xx} and (b) R_{xy} versus V_g at $B = 11$ T and $I_{bias} = 0$ nA (black), 17 nA (red) and 86 nA (blue). The V_g ranges correspond to the regions of the $\nu = \pm 2$ plateaux; see dotted line in (b). (c) The average fluctuations ΔR_{xx} and ΔR_{xy} versus I_{bias} , determined in the V_g range shown in (a) and (b). All data are measured at $T = 30$ mK.

of σ_{xy} . The transport gap gives rise to a strongly suppressed conductivity tensor in the low-density regime ($\sigma_{xx}, \sigma_{xy} \rightarrow 0$ if $R_{xx} \rightarrow \infty$; see [13]). Fig. 3a,b show that the transport gap disappears when we apply a sufficiently high bias, leading to non-vanishing values of σ_{xx} and σ_{xy} in the vicinity of the Dirac point. Moreover, in the high density regime, the fluctuations of σ_{xx} and σ_{xy} are suppressed at high bias, and the SdH oscillations of σ_{xx} and the quantization plateaux of σ_{xy} are more visible.

In order to investigate the origin of the reproducible fluctuations at low temperature, we analyze the fluctuations of R_{xx} and R_{xy} in the region of the $\nu = \pm 2$ Hall plateaux (since these are the best developed plateaux in our measurements). Fig. 4a,b show that the fluctuations (ΔR_{xx} , ΔR_{xy}) are smallest in the center region of the plateaux, whereas they increase strongly farther from the center region (i.e. in the transition regions between adjacent plateaux). The bias-dependence of ΔR_{xx} and ΔR_{xy} (Fig. 4a-c) shows that the fluctuations in the transition regions are strongly suppressed at $I_{bias} \gtrsim 10$ nA (this corresponds to $V_{bias} \gtrsim 100$ μ V, because $R_{xx} \sim 10$ k Ω in the transition regions; see dotted line in Fig. 4a).

Resistance fluctuations in the quantum Hall regime have been studied extensively in mesoscopic devices based on Si and GaAs heterostructures [17]. When the device dimensions are of the order of l_ϕ , phase coherent scattering mechanisms give rise to resistance fluctuations in the quantum Hall regime, similar to universal conductance fluctuations in the zero-field regime [18]. Since our nanoribbon dimensions are of the order of l_ϕ , the ob-

served resistance fluctuations may originate from quantum interference. Fig. 4c shows indeed that the fluctuations are suppressed on an energy scale of $\sim 100 \mu\text{eV}$, which is of the same order as the Thouless energy of the ribbon ($E_{Th} = \hbar D/L^2 \approx 100 \mu\text{eV}$). This also explains why these fluctuations are suppressed at 4.2 K, when $kT > E_{Th}$. Thus, our results indicate that the observed fluctuations in the quantum Hall regime can be mainly attributed to phase coherent scattering mechanisms in the disordered graphene nanoribbon.

In conclusion, we have measured the quantum Hall effect in a 60 nm wide graphene nanoribbon, which results in the observation of SdH oscillations of σ_{xx} and quantized plateaux of σ_{xy} for $\nu = \pm 2, \pm 6$ and ± 10 . At $T = 30$ mK, we observe large fluctuations of σ_{xx} and σ_{xy} at high charge densities, which may be attributed to phase coherent scattering mechanisms in the ribbon. At low charge densities, the electrons are confined in the ribbon yielding a transport gap, in which transport is dominated by charging effects. Since the transport gap does not disappear in the quantum Hall regime, a bandgap due to lateral confinement cannot play a crucial role in the occurrence of the transport gap at high magnetic field (which confirms what has been reported before [5, 6]).

We thank H. Hettmansperger, J. Schelter and B. Trauzettel for useful discussions. This work was financially supported by the German research foundation DFG [DFG-JST joint research program 'Topological Electronics'], and the EU ECR Eurocores programme [Eurographene project].

* Electronic address: jeroen.oostinga@physik.uni-wuerzburg.de

- [1] K. S. Novoselov *et al.*, Nature **438**, 197 (2005); Y. Zhang, Y. W. Tan, H. L. Stormer & P. Kim, Nature **438**, 201 (2005)
- [2] F. Molitor *et al.*, J. Phys.: Condens. Matter. **23**, 243201 (2011)
- [3] K. Nakada, M. Fujita, G. Dresselhaus & M. S. Dresselhaus, Phys. Rev. B **54**, 17954 (1996); L. Brey & H. A. Fertig, Phys. Rev. B **73**, 235411 (2006); Y. W. Son, M. L. Cohen & S. G. Louie, Phys. Rev. Lett. **97**, 216803 (2006)
- [4] M. Fujita, K. Wakabayashi, K. Nakada & K. Kusakabe, J. Phys. Soc. Jap. **65**, 1920 (1996); Y. W. Son, M. L. Cohen & S. G. Louie, Nature **444**, 347 (2006), A. Rycerz, J. Tworzydło & C. W. J. Beenakker, Nat. Phys. **3**, 172 (2007); B. Trauzettel, D. V. Bulaev, D. Loss & G. Burkard, Nat. Phys. **3**, 192 (2007)
- [5] D. Gunlycke, D. A. Areshkin & C. T. White, Appl. Phys. Lett. **90**, 142104 (2007); A. Lherbier, B. Biel, Y. M. Niquet & S. Roche, Phys. Rev. Lett. **100**, 036803 (2008); M. Evaldsson, I. V. Zozoulenko, H. Xu & T. Heinzl, Phys. Rev. B **78**, 161407 (2008); D. Querlioz *et al.*, Appl. Phys. Lett. **92**, 042108 (2008); E. R. Mucciolo, A. H. Castro Neto & C. H. Lewenkopf, Phys. Rev. B **79**, 075407 (2009); I. Martin & Y. M. Blanter, Phys. Rev. B **79**, 235132 (2009)
- [6] M. Y. Han, J. C. Brant & P. Kim, Phys. Rev. Lett. **104**, 056801 (2010); J. B. Oostinga, B. Sacépé, M. F. Craciun & A. F. Morpurgo, Phys. Rev. B **81**, 193408 (2010)
- [7] C. Stampfer *et al.*, Phys. Rev. Lett. **102**, 056403 (2009); K. Todd, H. T. Chou, S. Amasha & D. Goldhaber-Gordon, Nano Lett. **9**, 416 (2009); P. Gallagher, K. Todd & D. Goldhaber-Gordon, Phys. Rev. B **81**, 115409 (2010)
- [8] N. M. R. Peres, A. H. Castro & F. Guinea, Phys. Rev. B **73**, 195411 (2006); L. Brey & H. A. Fertig, Phys. Rev. B **73**, 195408 (2006)
- [9] Y. M. Lin, V. Perebeinos, Z. Chen & P. Avouris, Phys. Rev. B **78**, 161409 (2008); C. Lian *et al.*, Appl. Phys. Lett. **96**, 103109 (2010); N. Tombros *et al.*, Nat. Phys. **7**, 697 (2011)
- [10] R. Ribeiro *et al.*, Phys. Rev. Lett. **107**, 086601 (2011); S. Minke *et al.*, Phys. Rev. B **85**, 195432 (2012); H. Hettmansperger *et al.*, arXiv:1205.5144 (2012)
- [11] The value of C_g is obtained from Hall measurements at different V_g . The gate-dependence of the Hall coefficient is $R_H = R_{xy}/B = 1/en = 1/C_g(V_g - V_g^D)$, resulting in $C_g \approx 210 \mu\text{F}/\text{m}^2$.
- [12] A. F. Morpurgo & F. Guinea, Phys. Rev. Lett. **97**, 196804 (2006); F. V. Tikhonenko, D. W. Horsell, R. V. Gorbachev & A. K. Savchenko, Phys. Rev. Lett. **100**, 056802 (2008)
- [13] First the longitudinal magnetoresistance data is symmetrized, $R_{xx}^s(B) = \frac{R_{xx}(+B) + R_{xx}(-B)}{2}$, and the Hall data is antisymmetrized, $R_{xy}^a(B) = \frac{R_{xy}(+B) - R_{xy}(-B)}{2}$. Then the conductivity tensor values are determined: $\sigma_{xx} = \frac{\rho_{xx}}{\rho_{xx}^2 + \rho_{xy}^2}$ and $\sigma_{xy} = \frac{\rho_{xy}}{\rho_{xx}^2 + \rho_{xy}^2}$ with $\rho_{xx} = R_{xx}^s W/L$ and $\rho_{xy} = R_{xy}^a$.
- [14] E. McCann *et al.*, Phys. Rev. Lett. **97**, 146805 (2006)
- [15] The LL energy sequence of Dirac fermions in graphene is [1]: $E_N = \text{sgn}(N)\sqrt{2e\hbar v_f^2|N|B}$ with $N = 0, \pm 1, \pm 2, \dots$. The $\nu = \pm 4(|N| + 1/2) = \pm 2, \pm 6$ and ± 10 plateaux occur when the $N = 0, \pm 1$ and ± 2 LLs are near complete filling, respectively (note that positive/negative indices account for electron/hole states). Thus, at $B = 11$ T, the LL spacings corresponding to the $|\nu| = 2, 6, 10$ plateaux are 117 meV, 49 meV and 37 meV, respectively.
- [16] The zero-energy LL ($N = 0$) of graphene consists of electron and hole states [1]. This LL therefore closes a bandgap between electron and hole states, which may be present due to lateral confinement. If a size quantization gap would play a crucial role in the electron localization mechanism of our ribbons, then the electrons would delocalize when this gap is closed at high magnetic field.
- [17] P. C. Main *et al.*, Phys. Rev. B **50**, 4450 (1994); D. H. Cobden, C. H. W. Barnes & C. J. B. Ford, Phys. Rev. Lett. **82**, 4695 (1999); T. Machida, S. Ishizuka, S. Komiyama, K. Muraki & Y. Hirayama, Phys. Rev. B **63**, 045318 (2001); F. Hohls, U. Zeitler & R. J. Haug, Phys. Rev. B **66**, 073304 (2002); E. Peled, D. Shahar, Y. Chen, D. L. Sivco & A. Y. Cho, Phys. Rev. Lett. **90**, 246802 (2003)
- [18] C. W. J. Beenakker & H. van Houten, Solid State Phys. **44**, 1 (1991); M. Büttiker, Semicond. Semimetals **35**, 191 (1992)